Defence Science Journal, Vol. 73, No. 2, March 2024, pp. 163-172, DOI : 10.14429/dsj.74.19623

Investigation of Transonic Flow Features in an Axial Flow Compressor Rotor

Lakshya Kumar[#,*], Dilipkumar B. Alone[#], A.M. Pradeep[$], M.T. Shobhavathy[#] and Satish Kumar S.[#]

[#]*Propulsion Division, National Aerospace Laboratories, Bangalore – 560 017, India*
[$]*Department of Aerospace Engineering, Indian Institute of Technology Bombay, Mumbai – 400 076, India*
[*]*E-mail: lakshyakumar@nal.res.in*

ABSTRACT

Numerical investigation of an axial flow rotor is carried out for its performance characterization and aerodynamic behavior during the design and off-design operating conditions. The study focuses on capturing the transonic flow features from the choke point (CP) to the near stall (NS) point in the rotor. This includes the analysis of passage shock structure, its movement in the blade passage with varying back-pressure, shock boundary layer interaction, tip leakage flow structure, and resulting losses. The study is carried out from 60 % to 100 % of the design speed using steady and unsteady RANS simulations. Three turbulence models, namely; SST, k-ε, and Reynolds stress models, are employed. The SST model predicted the closest approximation to the experimental data. The rotor aerodynamic performance is predicted in terms of total pressure ratio, efficiency, and flow contours. Unsteady analysis revealed that the primary and secondary tip leakage vortices, combined with the suction side tip corner separation, are the major instabilities near the stall region.

Keywords: Transonic; Rotor; Tip-leakage flow; Shock-boundary layer interaction

NOMENCLATURE

BL : Boundary layer
BPF : Blade passing frequency (Hz)
C : Blade chord
C_p : Coefficient of pressure $C_p = \frac{P_2 - P_1}{P_{o1} - P_1}$
CP : Choke point
LE : Leading edge
M_{rel} : Relative Mach number
$m_{corrected}$: Corrected mass flow (kg/s)
N : Rotational speed (rpm)
η : Efficiency (%)
P_o : Total pressure (Pa)
P_{atm} : Standard atmospheric pressure (Pa)
PE : Peak efficiency
PR : Pressure ratio
PS : Pressure surface
RANS : Reynolds averaged navier stokes
SS : Suction surface
TE : Trailing edge
TLF : Tip leakage flow
P_1, P_2 : Static pressure at the inlet and blade surface (Pa)

1. INTRODUCTION

High-speed compressor rotors have the potential to generate higher pressure ratio and efficiency with a minimum number of stages enabling significant weight reduction. However, the rotor speed is constrained by the strong shock structures encountered in the blade passage. The strong shock system, in combination with tip leakage flow (TLF), is of significant concern within the gas turbine fraternity, as it contributes to around 30 % of the passage losses[1-3]. The interaction of tip leakage flow with the incoming core flow is one of the prominent sources of the stall inception in the tip critical rotor[4-5]. Therefore, understanding their genesis is crucial to curtailing the passage secondary losses and tip leakage flow.

There are enormous efforts put in by many researchers to suppress the dominance of passage shock and TLF, such as; Sunder[6-7], *et al.*investigated the effect of TLF and passage shock interaction on rotor performance. The study showed the blockage in the tip region is essentially due to the blade boundary layer separation caused by passage shock and TLF interaction. Gerolymos[8], *et al.* numerically analyzed the tip clearance flow and consequent secondary losses using various turbulence models. It was found that the overall performance prediction was well matched with experiments; however, hub corner separation and tip mixing regions were difficult to capture numerically. Hah[9], *et al.* carried out the unsteady analysis of the near casing flow of a forward-swept transonic rotor. The study was focused on analyzing the role of TLF, passage shock, and casing boundary layer interaction in stall inception. It was reported that tip leakage vortices do not break despite the rotor approaching stall, and the flow field unsteadiness was majorly due to the shock oscillations. Contrary to this, the study by Yamada[10], *et al.* showed that tip leakage vortices do break due to interaction with the passage shock and create significant flow blockage near the tip region.

Hah[11], *et al.* investigated the 3D shock structure, shock boundary layer interaction, radial mixing, wake development,

Received : 14 November 2023, Revised : 05 January 2024
Accepted : 12 January 2024, Online published : 26 March 2024

and flow separation in a transonic rotor. The study reported that the shock system induced flow separation above 60 % of the blade span, and below 60%, the separation was due to the usual pressure gradient. In the separation region, the strong radially outward motion of the flow was also reported. Biollo[12], *et al.* explored the effect of shock/boundary layer interaction in a three-dimensionally stacked rotor. It was found that the new rotor had higher efficiency and the same pressure ratio compared to the baseline one. Modified stacking helped to reduce the shock losses and improved the flow field in the end wall region.

Yongzhen[13], *et al.* employed a Shock Control Bump (SCB) on the suction surface of a transonic rotor. It was observed that above 95 % of design speed, SCB breaks the strong shock into two weak shocks and reduces the flow separation; however, SCB was not very effective below design speed. Juan[14], *et al.* studied the flow structure within the tip region of a transonic rotor capturing 2D and 3D shock structure, expansion wave around the leading edge, and tip leakage flow. The study pointed out two observations; (i) There is an interface between incoming core flow and TLF, and (ii) Based on blade loading, there exist two components of TLF along the blade chord, and each of them contributes differently to stall inception.

Zinon[15] extensively assessed the effectiveness of various turbulence models for predicting transitional flows on a double circular arch compressor blade. Based on the outcome, it was found that for accurate prediction of complex flow fields encountered in compressors, unsteady Reynolds averaged Navier Stoke or hybrid simulation having an unsteady approach is required.

The present investigation is aligned in a similar direction to investigate the transonic flow features such as shock structure, tip leakage flow, and shock boundary layer interaction in an axial flow rotor. This transonic rotor is part of a research compressor stage at the Propulsion Division, CSIR-NAL[16-17]. The technical details are given in Table 1.

Table 1. Technical specifications of the rotor

Parameter	Value
No of Blades	21
Speed	13250 (rpm)
Tip relative Mach No	1.15
Tip diameter	451 (mm)
Corrected mass flow	23 (kg/s)
Pressure ratio (PR)	≈1.45
Inlet hub tip ratio	0.518
Tip speed	305 (m/s)
Rotor tip Chord	84 (mm)

2. GEOMETRY MODELING, MESHING, AND NUMERICAL SOLVER

The rotor geometry considered is a 17.14° sector single-blade passage. The inlet and outlet domain was extended by 1×C and 3×C, respectively. A rotor tip clearance of 0.55 mm was provided. The computational domain of the rotor is illustrated in Fig. 1(a). Geometry meshing was carried out using Turbogrid with a combination of O and H topology around the blade to create hexahedral elements throughout the domain, as shown in Fig. 1(b). The first element size near the solid wall was made small enough to meet the Y^+criterion required for the turbulence model.

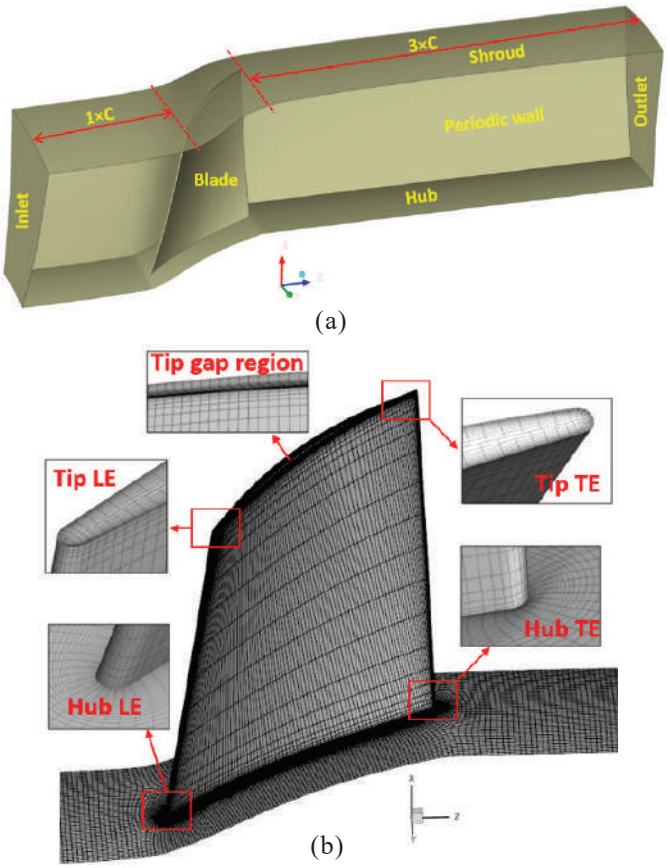

Figure 1. (a) Rotor domain with the boundary conditions; and (b) Mesh generated for the rotor.

The inlet boundary of the compressor was treated as a pressure inlet, while the exit boundary as a pressure outlet. The side boundaries were defined as rotationally periodic, while the hub and shroud as no-slip walls. To ensure the reliability of the numerical predictions, grid independent study was carried out for 0.28, 0.55, 0.74, and 1.1 million mesh sizes monitoring peak total pressure rise (ΔP_o). The difference between the 0.74 and 1.1 million was 0.16 % which is negligible, and the predictions became almost similar, as is evident from Fig. 2. Therefore the mesh size of 1.1 million was considered for all further analysis. Steady and unsteady RANS numerical simulations have been carried out using a commercial CFX solver. A cell-centered finite volume approach is considered. The second-order upwind scheme (high-resolution) is chosen for the numerical discretization. Three turbulence models, namely; SST, k-ε, and Reynolds stress, are adopted for the turbulence closure.

3. ROTOR PERFORMANCE CHARACTERIZATION

The rotor performance is characterized in terms of total pressure ratio and isentropic efficiency, as shown in Fig. 3(a) and Fig. 3(b). The circular dots represent the experimental values[18-19], and the solid lines represent numerical predictions. The pressure ratio (PR) and efficiency are slightly over-

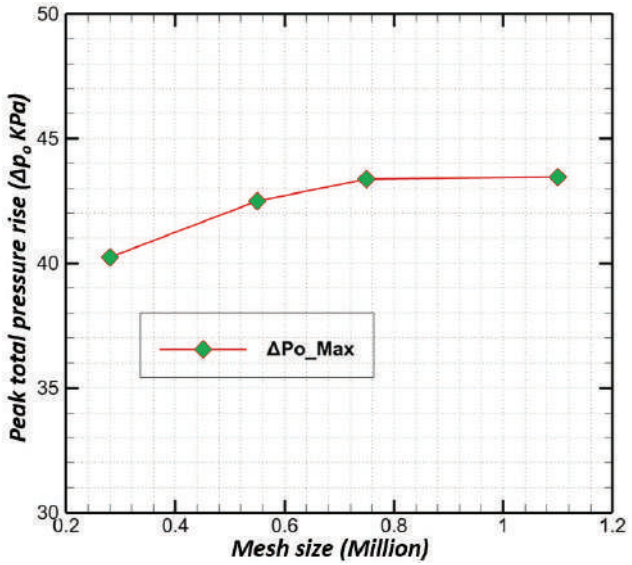

Figure 2. Non-dimensional exit total pressure and mass flow variation for different mesh sizes.

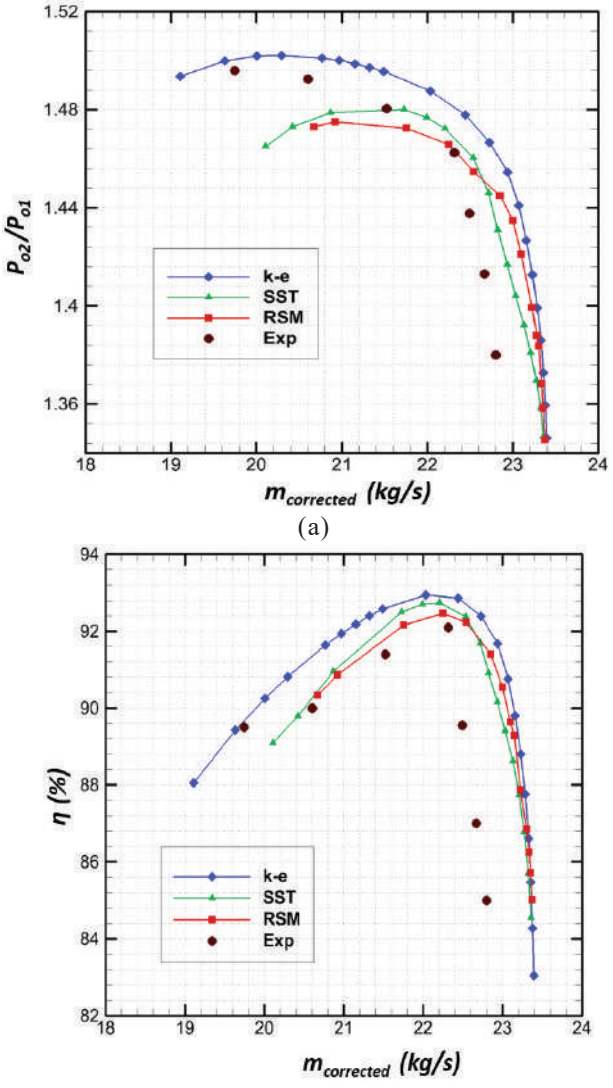

Figure 3. (a) Pressure ratio (PR) versus corrected mass flow at 100 % speed; and (b) Efficiency versus corrected mass flow at 100 % speed.

predicted from the choke to the near stall region; however, the performance trend is well followed by all the turbulence models. Apparently, the SST model shows the closest approximation for PR, Efficiency, and, more importantly, the near stall mass flow predictions. Therefore, the off-design performance characterization at various speeds is carried out for the SST model and presented in Fig. 4(a) and Fig. 4(b).

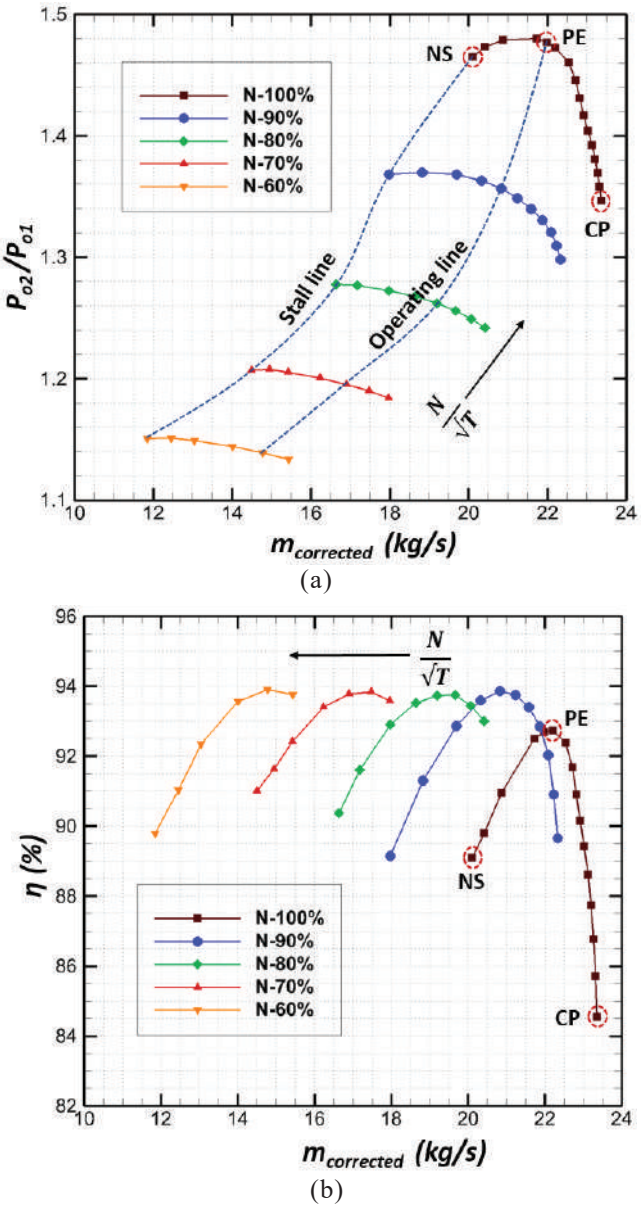

Figure 4. (a) PR versus corrected mass flow characteristics at various speeds; and (b) Efficiency versus corrected mass flow characteristics at various speeds.

In the numerical simulations, the onset of the stall is considered at a point where the solution diverges with increasing back pressure. This point is defined as a Near-Stall (NS) point. At 100 % of the design speed, the rotor operates in the high transonic regime, which can be interpreted from the PR and efficiency versus corrected mass flow characteristics being very steep from the Choke Point (CP) to the Peak Efficiency (PE) point. At high transonic conditions, the compressor tip region encounters supersonic Mach numbers causing shock

losses and consequent aerodynamic instabilities. This results in lower peak efficiency and reduced stall margin. On the other hand, at 90 % of speed, the tip Mach number is relatively lower; correspondingly, the shock losses too. This helps to achieve higher peak efficiency and stall margin. With speed falling below 80 %, the rotor operates in a subsonic regime, exhibiting almost flat PR characteristics and a large variation of mass flow between CP and NS conditions.

4. ROTOR FLOW FEATURES

The various flow features of the rotor for CP, PE, and NS points at the hub, mean, and tip sections are presented with the help of relative Mach (Mrel) contours in Fig. 5(a), (b), and (c) and are marked with the white dashed line in the respective figures. At the choke point, the blade incidence is almost zero; therefore, as the flow approaches the blade leading edge, the streamline gets deflected around the blade Pressure Surface (PS) and Suction Surface (SS). At this point, neither the blades are fully loaded, nor the back pressure is very high; hence the flow accelerates in the blade passage leading to a supersonic Mach number upon the blade surface on either surface. This results in the formation of strong shocks on the Suction Surface (SS) and Pressure Surface (PS). The shock Boundary Layer (BL) interaction at the suction surface makes the flow separate from the surface. The pressure rise across the shock is so high that it can cause the boundary layer to separate a little

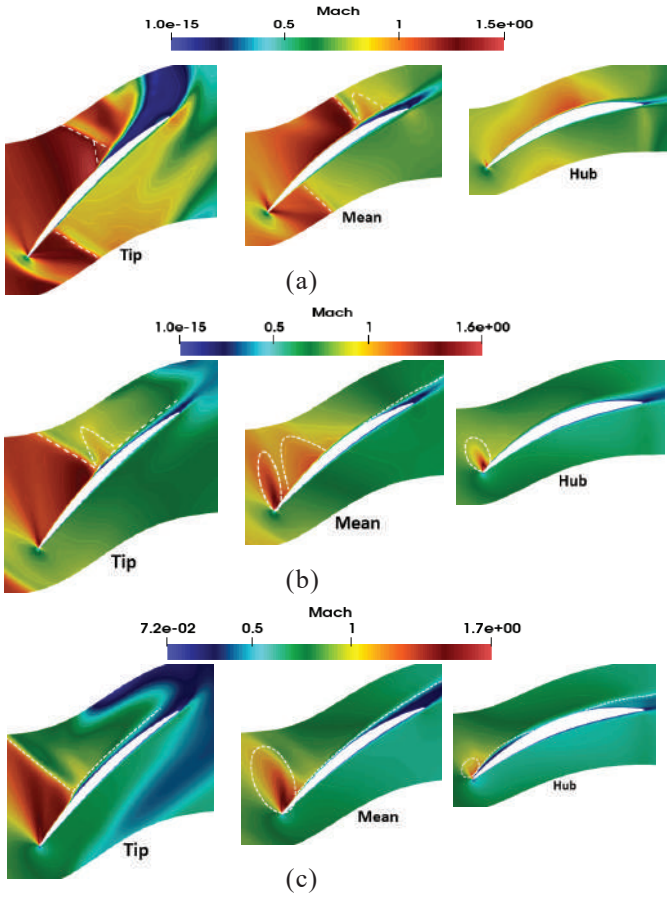

Figure 5. (a) Relative Mach number contours at Choke point; (b) Relative Mach number contours at peak efficiency point; and (c) Relative Mach number contours at near stall point.

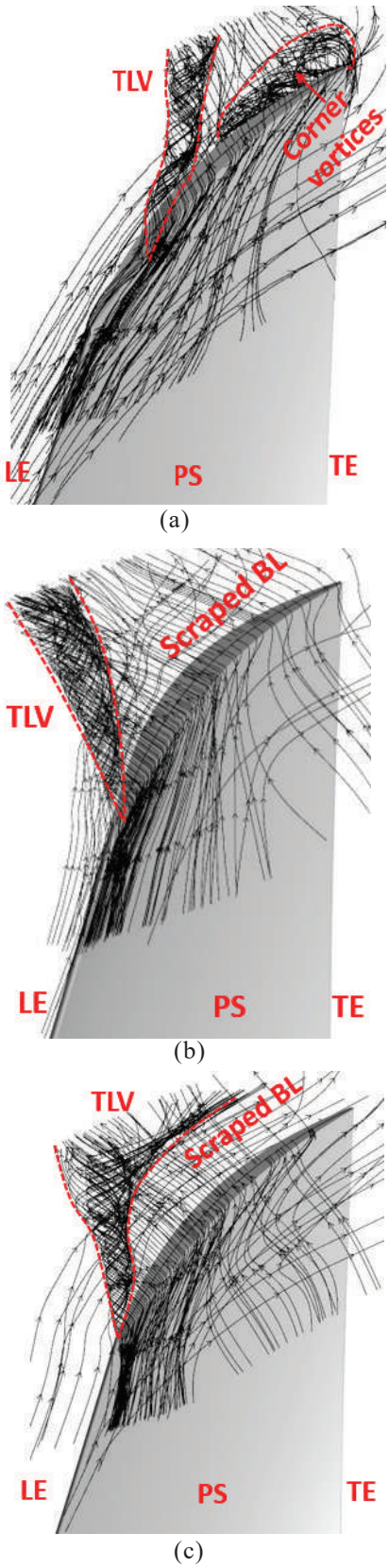

Figure 6. (a) Streamline pattern in the rotor tip region for CP at 100 % speed; (b) Streamline pattern in the rotor tip region for PE at 100 % speed; and (c) Streamline pattern in the rotor tip region for NS at 100 % speed.

upstream of the shock. Consequently, there is a sudden change in the direction of the core flow, accompanied by an oblique

shock interacting with the main shock and creating a lambda shock structure. The pressure surface shock boundary layer interaction does not cause flow separation; this is attributed to the weak interaction. The shock emanating from the pressure side also interacts with the adjacent blade-separated boundary layer; however, it does not show any severe effect due to the weak nature of the interaction. The prevailing supersonic Mach number at the mean section also results in shock formation on the suction and pressure side. Here, the shock boundary layer interaction at the SS is weak; hence the severity of flow separation is also reduced. A local acceleration bubble can be observed just downstream of the shock and adjacent to the separated boundary layer due to the radial migration of the hub accelerating flow. The hub section has a rapid acceleration near the leading edge (LE) followed by a gradual one at the suction side. Overall the hub section flow is high subsonic without any severe flow separation.

At the PE point, rotor blades are optimally loaded, and as the flow goes around the blade, it keeps accelerating on the suction surface, forming a normal shock. The interaction between the blade boundary layer and the shock causes the flow to separate; however, the boundary layer is still well-behaved. A leading edge shock is formed at the mean section, followed by a local accelerating bubble extending radially up to the tip. At the hub, majorly the flow is subsonic except for the leading edge acceleration with a weak shock. The flow separation at the mean and hub is not very significant.

At the NS point, aerodynamic instabilities in the rotor increase, making the flow highly unsteady. The accelerating flow at the tip suction surface creates a strong normal shock which is shifted upstream due to high back pressure. Also, the increasing streamwise pressure gradient makes the blade BL to be thick. The interaction between this thick boundary layer and the shock causes severe flow separation, which is asymmetric in nature due to the combined influence of radial and streamwise pressure gradients. At the mean section also, flow undergoes rapid acceleration from the LE over the SS and shock-induced separation. The hub flow accelerates over the SS near the LE. This acceleration leads to a very weak leading edge shock and consequent flow separation. The flow re-attaches to the blade surface and again separates from the blade; due to the trailing edge separation and blade hub corner separation.

The Tip Leakage Flow (TLF) is a pressure-driven phenomenon that is inherently associated with the rotor. This tip leakage flow interacts with the core flow and generates a significant amount of secondary losses in the tip region. The intensity of TLF increases with the increasing pressure difference between the blade pressure and suction surface; Fig. 6(a), (b), and (c) show the TLF streamline pattern at CP, PE, and NS points, respectively. The TLF consists of several vortex structures rotating in the direction opposite to rotor rotation and is collectively called Tip Leakage Vortex (TLV). At the CP, the TLV emanates a little downstream of the leading edge as the flow accelerates on the pressure and suction surface. After the occurrence of normal shock at the pressure surface, a significant pressure difference is created, and TLV is formed. A remarkable corner vortices can also be seen on the suction surface near the trailing edge, which is attributed

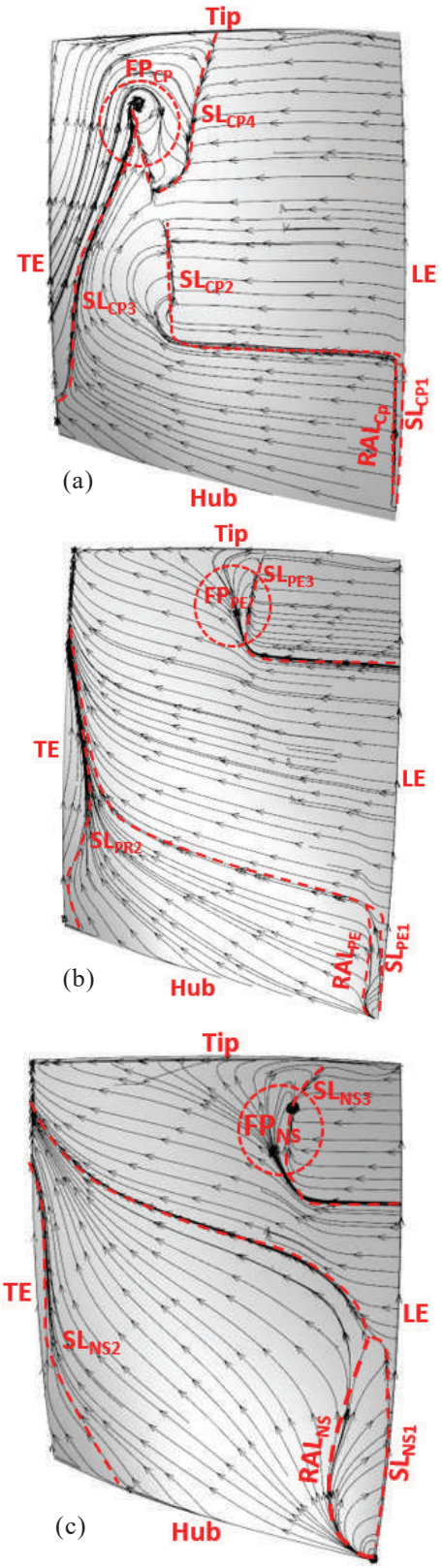

Figure 7. (a) Surface shear line at rotor suction surface for CP at 100 % speed; (b) Surface shear line at rotor suction surface for PE at 100 % speed; and (c) Surface shear line at rotor suction surface for NS at 100 % speed.

to the significant corner separation in the tip region. The TLV becomes very intense at the PE point and moves away from the blade in a very concentrated manner. Due to the increased

aerodynamic instabilities at the NS point, the TLV becomes unstable and widens towards the end. This widened TLV strikes on the adjacent blade PS and gets mixed with the core flow.

The suction surface shear lines developed at the blade for CP, PE, and NS are illustrated in Fig. 7(a), (b) and (c). All the separation lines (SL) and reattachment lines (RAL) are marked by red dashed lines, and zone-wise specific numbering is provided. At the CP, there is a local leading-edge flow separation (SL_{CP1}) and immediate reattachment (RAL_{CP}) in the hub region caused by weak LE shock. The separation lines SL_{CP2}in the midsection and SL_{CP4}in the tip section are also due to shock and blade boundary layer interaction. Near the tip, there is a focal point (FP marked by a red circle) of recirculation developed due to the corner flow separation. This has caused the trailing edge separation (SL_{CP3}) to extend radially down up to 90% of the span. The leading edge separation (SL_{PE1}) and reattachment (RAL_{PE}) zone for PE is a little widened compared to CP near the hub. The shock-induced separation zone (SL_{PE3}) near the tip region is very sharp, followed by a recirculation zone (FP_{PE}). The trailing edge separation (SL_{PE2}) is also not very severe; however, a radial drifting of the flow from the hub can be observed. The zone of leading edge separation (SL_{NS1}) and reattachment (RAL_{NS}) is very large for the NS condition. The tip separation (SL_{NS3}) is extended radially down and moved upstream due to the shock movement. The hub corner separation has increased the extent of trailing edge separation (SL_{NS2}) and radial migration of the hub flow.

In a transonic rotor, the blade loading varies significantly at the hub, mean, and, specifically, tip sections due to passage shock and TLF. This variation is presented in the form of the coefficient of pressure for C_p, PE, and NS conditions in Figures 8 (a), (b), and (c). For the choke point, tip $C_p$variation on the pressure surface and suction surface crosses at around 18% of the blade chord on either side due to flow acceleration.

The suction side C_p keeps decreasing till 45 % of the chord, followed by a sudden increase caused by the shock. The pressure surface shock occurs at around 15 % of the chord, causing a sudden rise in C_p afterward. The C_p line also crosses at the mean section; however, the pressure and suction surface shock locations are at around 58 % and 18 % of the chord, respectively.

For the PE point (Fig. 8 (b)), tip C_p variation over the suction surface can be observed as decreasing from the leading edge to 35 % of the chord and then a sudden rise caused by the shock. Conversely, the pressure side C_p keeps rising steadily over the entire surface. The mean section C_p also reduces slightly due to leading-edge acceleration and rises afterward due to the occurrence of shock. A weak shock at the hub leading edge causes a steep rise in C_p, followed by a very gradual rise over the pressure and suction surface throughout the blade chord. The near-stall C_p variation at all three sections follows a similar trend as PE; however, the location of shock occurrence is significantly different. As can be seen in Fig. 8 (c), the tip chock is moved upstream at around 15 % of the chord due to increased back pressure.

The pitch-wise total pressure at the rotor exit for PE and NS is shown in Fig. 9 (a), (b), and (c). The rotor pressure ratio begins to build up from the choke point, but as it's not a design

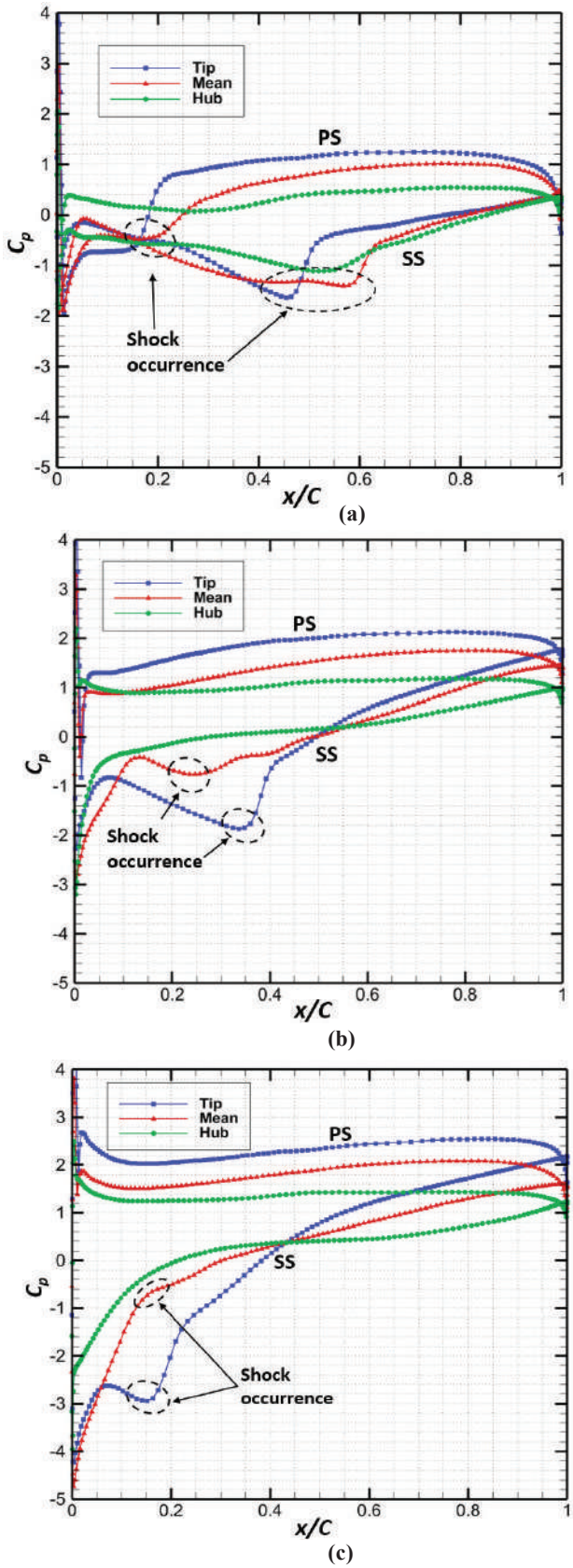

Figure 8. (a) Coefficient of pressure at the hub, mean, and tip for choke point (100 % speed); (b) Coefficient of pressure at the hub, mean, and tip for peak efficiency point (100 % speed); and (c) Coefficient of pressure at the hub, mean, and tip for near stall point (100 % speed).

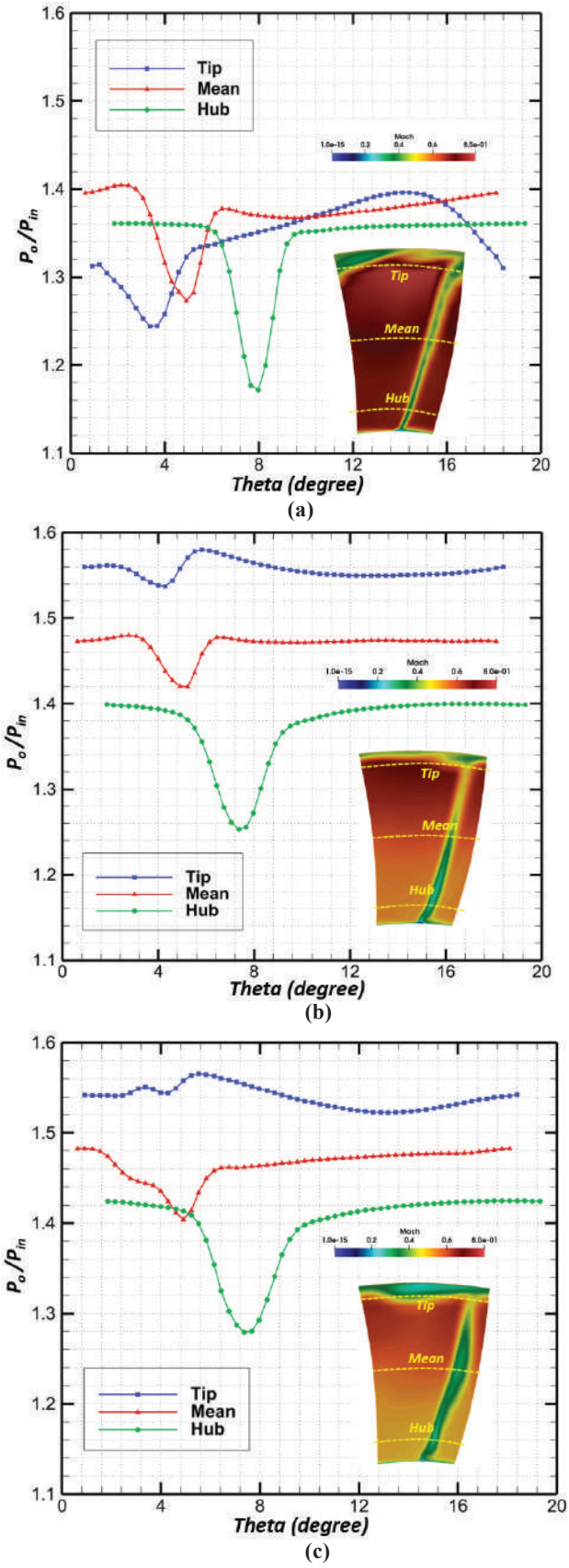

Figure 9. (a) Pitch-wise total pressure at rotor exit for choke point (100 % speed); (b) Pitch-wise total pressure at rotor exit for peak efficiency point (100 % speed); and (c) Pitch-wise total pressure at rotor exit for near stall point (100 % speed).

point, the large fluctuations in the pitch-wise pressure are very obvious. Here at the CP, the total pressure fluctuations in the tip region are significant due to the corner-separated flow and unstable casing boundary layer. The flow disturbances keep dampening out towards the hub, which can be seen at the mean and hub total pressure being almost constant over the pitch except for one V-shaped dip due to the blade trailing edge wakes.

At the PE point, the losses in the blade passage are relatively lower, and the boundary layer at the blade is also well-behaved. This is reflected in terms of almost constant total pressure at the tip, mean, and hub with only dip due to the blade trailing edge wake. Towards the stall, the flow instabilities increase, resulting in the total pressure loss as seen at the NS point. The tip region being dominated by tip leakage flow results in large fluctuations and loss of total pressure. At the mean section, a small fluctuation can be seen; however, the hub total pressure is almost constant away from the blade trailing edge zone.

5. UNSTEADY ANALYSIS OF THE ROTOR NEAR STALL

The unsteady simulation of the rotor flow physics is carried out at the NS point. The steady-state RANS solution corresponding to the NS point is taken as the initial value. Ten rotor revolutions are defined in the simulation. The single-blade passing period is calculated as the time taken by the rotor blade to pass the one pitch of the stator blade. Each passing period is divided into 20-time steps corresponding to a size of 1.19×10^{-5}seconds. The total time steps for the ten revolutions are 4200, which is found to be adequate to achieve a converged solution. The time history of the static pressure signal is monitored, and as the periodicity of the pressure signal becomes repetitive in nature, the solution is considered to be converged. Figure 10 shows the static pressure signals captured at the blade trailing edge and the corresponding Fourier transform, giving the first, second, and third harmonics of the Blade Passing Frequency (BPF). Here the frequency is non-dimensionalized by the 4638 Hz, which corresponds to the rotor BPF.

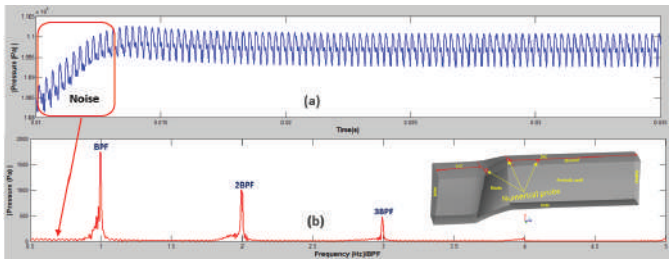

Figure 10. (a) Time history of the static pressure signals and corresponding; and (b) FFT showing blade passing frequencies.

The dominant vortex structures in the rotor passage before the onset of stall are Primary Tip Leakage Vortex (P-TLV), Secondary Tip Leakage Vortex (S-TLV), vortex due to Shock Boundary Layer Interaction (SBL-V), leading-edge spillage vortex (SV), suction side corner vortex (H-CV) at the hub, Horseshoe Vortex (HSV) near the hub leading edge, ramp

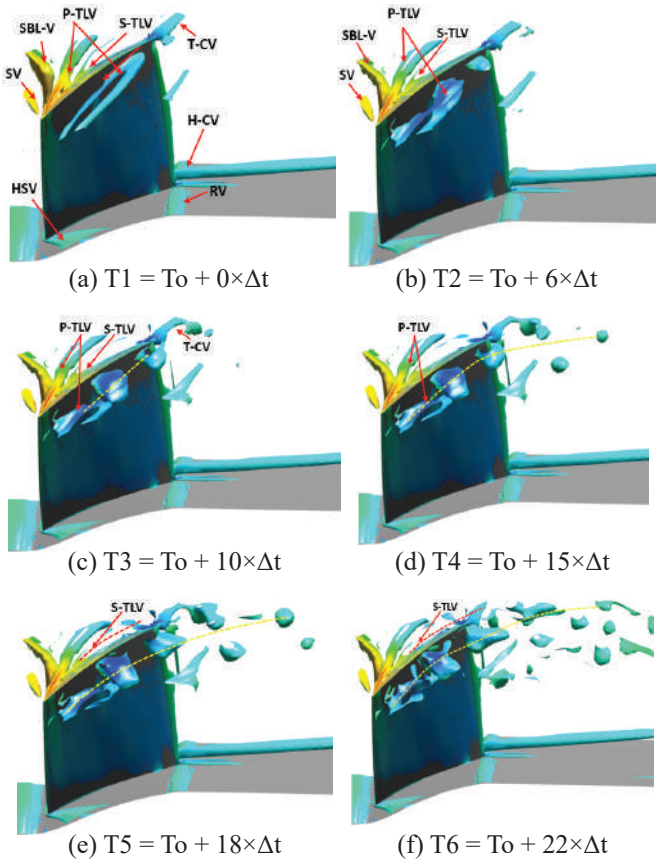

Figure 11. Instantaneous iso-surfaces showing the various secondary flow structures in the rotor domain near stall condition at different time instances (Q-criterion 10×E-4).

vortex due to hub contour and tip corner vortex, all of them are marked in Fig. 11(a). Most of these vortex structures are inherent; however, their frequency and magnitude depend on the blade passing frequency and downstream back pressure for a particular speed and inlet conditions. The primary sources of rotor tip instability are; tip leakage vortex (TLV), tip corner vortices (T-CV), and other secondary flow structures. At stable operating conditions, TLV is confined in the close vicinity of the blade, creating one single oval-shaped vortex in the passage (Fig 11(a). With increasing back pressure, the TLV grows in size, and it becomes unstable to an extent where it starts breaking into two to three vortices (Fig. 11(b) and (c)). From this point, any incremental rise in the back pressure causes the breaking of the primary P-TLV. The S-TLV also interacts with the tip corner vortices (T-CV) near the trailing edge (trajectory shown by the red dotted line Fig. 11(e) and (f)). The primary P-TLV and the S-TLV, along with T-CV, get mixed near the blade trailing edge and break into multiple vortex structures, creating around 30 % blockage at the rotor exit. This eventually leads the rotor into the stall region.

6. CONCLUSIONS

Flow physics of a transonic rotor is investigated using a steady and unsteady Reynolds averaged Navier Stokes (RANS) solver. The analysis is carried out for various speeds and focused on choke point (CP), peak efficiency (PE) point, and near stall (NS). Out of SST, k-ε, and Reynolds stress models, the SST model gave the closest approximation to the experimental data specifically predicting the stall point mass flow (2 % difference in stall mass flow).

At transonic speed, the shock boundary layer interaction in combination with TLF creates higher losses in the tip region. The band of shock movement in the upstream direction is between 45 % to 18 % from CP to NS. The tip shock structure is very complex at the choke point due to the formation of lambda shock, whereas at PE and NS only a normal shock is formed. At 100 % of design speed, the span-wise (radially down) dominance of supersonic flow is 40 %, 25 %, and 30 % for CP, PE, and NS, which causes the occurrence of shock and consequent flow separation. Leading edge acceleration from the hub (radially up) has caused a mild shock and resulted in separation and reattachment over the suction surface. The radial migration of flow near the hub is observed due to corner separation, which becomes significant at the NS. The interference of the TLV with the adjacent blade is not observed for CP and PE; however, it has significant interference with the adjacent blade pressure surface for NS. The pitch-wise total pressure losses are also high at CP and NS due to the combined effect of TLF and unstable casing boundary layer.

The unsteady analysis showed that the major source of rotor tip instabilities is primary and secondary tip leakage vortices. These vortices get mixed with the suction side tip corner separation and break into multiple numbers of small vortices. Around 30 % of blockage is created by the vortex breaking near the stall condition. Vortex structures near the hub such as ramp vortex (RV), horseshoe vortex (HSV), and suction side corner vortex near the hub (H-CV) grow very marginally with the onset of the stall and do not cause any severe flow instability.

REFERENCES

1. Du, J.; Lin, F.; Chen, J.; Nie, C. & Biela, C. Flow structures in the tip region for a transonic compressor rotor. *ASME. J. Turbomach*., 2013, **135**(3), 031012. doi: 10.1115/1.4006779
2. Zhang, B.; Mao, X.; Wu, X. & Liu, B. Effects of tip leakage flow on the aerodynamic performance and stability of an axial-flow transonic compressor stage. *MPDI, Energies.*, 2021, **14,** 4168. doi: 10.3390/en14144168.
3. Flaszynski, P.; Doerffer P. & Szwaba, R. Shock wave boundary layer interaction on suction side of compressor profile in single passage test section. *J. Therm. Sci.,* 2015, **24**, 510–515. doi: 10.1007/s11630-015-0816-9
4. Wang, H.; Wu, Y.; Wang, Y. & Deng, S. Evolution of the flow instabilities in an axial compressor rotor with large tip clearance: An experimental and URANS study, *Aeros. Sci. Technol.,* 2020, **96,** 105557. doi: 10.1016/j.ast.2019.105557.
5. Muller, M.W.; Schiffer, H.; Voges, M. & Hah, C.

Investigation of passage flow features in a transonic compressor rotor with casing treatments. *In* Proceedings of the ASME 2011 Turbo Expo: Turbine technical conference and exposition. Vol.7: Turbomachinery, Parts A, B, and C. Vancouver, British Columbia, Canada. June 6–10, 2011. pp. 65-75.
doi: 10.1115/GT2011-45364

6. Suder, K.L. Blockage development in a transonic axial compressor rotor. *ASME. J. Turbomach*., 1998; **120**(3), 465–476.
doi: 10.1115/1.2841741
7. Suder, K.L. & Celestina, M.L. Experimental and computational investigation of the tip clearance flow in a transonic axial compressor rotor. *ASME. J. Turbomach*., 1996, **118**(2), 218–229.
doi:10.1115/1.2836629
8. Gerolymos, G.A. & Vallet, I. Tip-clearance and secondary flows in a transonic compressor rotor. *ASME. J. Turbomach*., 1999, **121**(4), 751–762.
doi: 10.1115/1.2836729
9. Hah, C.; Rabe, D.C. & Wadia, A.R. Role of tip-leakage vortices and passage shock in stall inception in a swept transonic compressor rotor. *In* Proceedings of the ASME Turbo Expo 2004: Power for Land, Sea, and Air. Vol. 5: Turbo Expo 2004, Parts A and B. Vienna, Austria. June 14–17, 2004, pp. 545-555.
doi: 10.1115/GT2004-53867
10. Yamada, K.; Furukawa, M.; Nakano, T.; Inoue, M. & Funazaki, K. Unsteady three-dimensional flow phenomena due to breakdown of tip leakage vortex in a transonic axial compressor rotor. *In* Proceedings of the ASME Turbo Expo 2004: Power for Land, Sea, and Air. Vol. 5: Turbo Expo 2004, Parts A and B. Vienna, Austria. June 14–17, 2004, pp. 515-526.
doi: 10.1115/GT2004-53745
11. Hah, C. & Reid, L. A viscous flow study of shock boundary layer interaction, radial transport, and wake development in a transonic compressor. *ASME J. Turbomach*., 1992, **538**(114).
doi: 10.1115/1.2929177
12. Roberto, B. & Ernesto, B. Shock/Boundary Layer/Tip-Clearance Interaction in a Transonic Rotor Blade. AIAA *J. Propulsion Power*., 2009.
doi:10.2514/1.39541,
13. Yongzhen, Liu.; Wei, Z.;, Qingjun, Z.; Qiang, Z. & Jianzhong. Passage shock wave boundary layer interaction control for transonic compressors using bumps. *Chinese J. Aero*., 2020, **35**(2), 82-97.
doi: 10.1016/j.cja.2021.05.014.
14. Du, J.; Lin, F.; Chen, J.; Nie, C. & Biela, C. Flow structure in the tip region of a transonic compressor rotor. *ASME J. Turbomach*., 2013, **135**(3).
doi: 10.1115/1.4006779
15. Vlahostergios, Z. Performance assessment of reynolds stress and eddy viscosity model on a transitional DCA compressor blade. *Aerosp.,* 2018, **5**(4), 102.
doi:10.3390/aerospace5040102.
16. Kumar, L.; B Alone, D. & Pradeep, A.M. Aerodynamics of inter-spool duct under the influence of an upstream transonic compressor stage. *Aerosp. Sci. Tech*., 2023, **137**, 108282.
doi: 10.1016/j.ast.2023.108282.
17. Kumar, S.; Alone, D.B.; T, S.M.; Mudipalli Reddy, J.R.; Kumar, L.; Ganguli, R.; Kandagal, S.B. & Jana, S. Aerodynamic behavior of a transonic axial flow compressor stage with self-recirculating casing treatment, *Aerosp. Sci. Tech.,* 2021, **112**, 106587.
doi: 10.1016/j.ast.2021.106587
18. Lieblein, S.; Lewis, George W. & Sandercock, Donald M. Experimental investigation of an axial-flow compressor inlet stage operating at transonic relative inlet mach numbers I - over-all performance of stage with transonic rotor and subsonic stators up to rotor relative inlet mach number of 1. NACA RM E52A24, 1952.
19. Rafeeq, M.A.M.; Nagpurwala, Q.H. & Shivaramaiah, S. Numerical studies on the effect of gurney flap on aerodynamic performance and stall margin of a transonic axial compressor rotor. *In* Proceedings of the ASME 2014, Gas Turbine India Conference. New Delhi, India. December 15–17, 2014.
doi: 10.1115/GTINDIA2014-8130.

ACKNOWLEDGEMENT

The authors are thankful to the director CSIR-NAL and the Head Propulsion Division for providing the resources to carry out this work and allowing us to publish it.

CONTRIBUTORS

Mr Lakshya Kumar is a Senior Scientist at CSIR-National Aerospace Laboratories Bangalore. He is working in the area of compressor aerodynamics, inter-stage ducts, and turboprop air intakes and is currently involved in the civil aircraft program and continuous wind tunnel for axial compressor-related activities. In the current study, he has conceptualized this study and carried out CFD analysis and manuscript preparation.

Dr Dilipkumar B. Alone is a Senior Principal Scientist at CSIR-National Aerospace Laboratories Bangalore. He obtained his PhD from IIT Bombay with a specialization in turbomachinery aerodynamics. His research interest includes: Compressor casing treatments and turboprop power plants. He is currently involved in the turboprop engine test facility and civil aircraft program. In the current study: he has carried out the review and was involved in the manuscript preparation.

Dr A.M. Pradeep is a Professor in Aerospace Engineering at the Indian Institute of Technology Bombay. His broad area of research is in the field of Aircraft propulsion. His research interests include: Turbomachinery design and performance enhancement strategies, active and passive flow control, experimental aerodynamics, and flow visualization.
In the current study: he has carried out the review and was involved in the manuscript preparation also.

Mrs M.T. Shobhavathy is a Senior principal Scientist at CSIR-National Aerospace Laboratories Bangalore and the in-charge

of the Axial Flow Compressor Research Facility. Her research area is the aero-thermodynamics of aero-engine compressors. She is also a quality inspector for the Hansa-NG trainer aircraft. In the current study: she has carried out the review and was involved in the manuscript preparation.

Dr Satish Kumar S. is a Principal Scientist at CSIR-National Aerospace Laboratories Bangalore. He obtained his PhD from IISc Bangalore in the field of Aerospace engineering. His areas of research include: Aeroelasticity, fluid-structure interaction and turbomachinery aerodynamics. He is currently involved in the development of de-icing and anti-icing system for SARAS-Mk-II aircraft intake.
In the current study: he has carried out the geometry modeling, review, and manuscript writing.